Available online at www.sciencedirect.com
ScienceDirect
Journal of Power Sources 177 (2008) 177–183
JOURNAL OF POWER SOURCES
www.elsevier.com/locate/jpowsour

Physical and electrochemical properties of spherical $Li_{1+x}(Ni_{1/3}Co_{1/3}Mn_{1/3})_{1-x}O_2$ cathode materials☆

S.-H. Park [a,1], S.-H. Kang [a], I. Belharouak [a], Y.K. Sun [b], K. Amine [a,*]

[a] *Argonne National Laboratory, 9700 S. Cass Avenue, Argonne, IL 60439, USA*
[b] *Department of Chemical Engineering, Hanyang University, Seoul 133-791, South Korea*

Received 3 September 2007; received in revised form 15 October 2007; accepted 16 October 2007
Available online 26 October 2007

Abstract

A $(Ni_{1/3}Co_{1/3}Mn_{1/3})CO_3$ precursor with an uniform, spherical morphology was prepared by coprecipitation using a continuously stirred tank reactor method. The as-prepared spherical $(Ni_{1/3}Co_{1/3}Mn_{1/3})CO_3$ precursor served to produce dense, spherical $Li_{1+x}(Ni_{1/3}Co_{1/3}Mn_{1/3})_{1-x}O_2$ ($0 \le x \le 0.15$) cathode materials. These Li-rich cathodes were also prepared by a second synthesis route that involved the use of an M_3O_4 ($M = Ni_{1/3}Co_{1/3}Mn_{1/3}$) spinel compound, itself obtained from the carbonate $(Ni_{1/3}Co_{1/3}Mn_{1/3})CO_3$ precursor. In both cases, the final $Li_{1+x}(Ni_{1/3}Co_{1/3}Mn_{1/3})_{1-x}O_2$ products were highly uniform, having a narrow particle size distribution (10-μm average particle size) as a result of the homogeneity and spherical morphology of the starting mixed-metal carbonate precursor. The rate capability of the $Li_{1+x}(Ni_{1/3}Co_{1/3}Mn_{1/3})_{1-x}O_2$ electrode materials, which was significantly improved with increased lithium content, was found to be better in the case of the denser materials made from the spinel precursor compound. This result suggests that spherical morphology, high density, and increased lithium content were key factors in enabling the high rate capabilities, and hence the power performances, of the Li-rich $Li_{1+x}(Ni_{1/3}Co_{1/3}Mn_{1/3})_{1-x}O_2$ cathodes.

Keywords: Carbonate precipitation; $Li(Ni_{1/3}Co_{1/3}Mn_{1/3})O_2$; Lithium secondary batteries; Positive materials; Layered materials

1. Introduction

$LiCoO_2$ is the most widely used cathode material in commercial lithium secondary batteries because of its easy mass production and reliable rechargeability with respect to the Li-ion cells that power consumer electronics. However, the toxicity and high cost of cobalt pose major obstacles that will limit its application in large-scale batteries, such as those intended to power hybrid electric vehicles (HEVs). Recently, $Li(Ni_{1/3}Co_{1/3}Mn_{1/3})O_2$ material has been proposed as an alternative to $LiCoO_2$ cathode material, mainly because of the former's higher reversible capacity and enhanced thermal stability [1–5].

The need for mass production of this promising cathode material has suggested adoption of the solid-state reaction method, which has advantages over other methods, especially from the standpoint of economics. However, in the case of the $Li(Ni_{1/3}Co_{1/3}Mn_{1/3})O_2$ material, the solid-state reaction method has led to impure phases, with none providing satisfactory cell performance [6]. Therefore, new preparation methods that allow for a better cationic distribution control are needed in order to eliminate secondary phases and improve the electrochemical behavior of the phases obtained. For this purpose, the coprecipitation method has been widely adopted as a preferred method to obtain mixed transition-metal hydroxide precursors with spherical morphologies. However, mixed transition-metal hydroxides containing Ni, Co, and Mn simultaneously have been found to be unstable, because during or after the coprecipitation process the $Mn(OH)_2$ hydroxide can be easily segregated from the mixed

☆ The submitted manuscript has been created by Argonne National Laboratory ("Argonne"), which is operated by UChicago Argonne, LLC, Argonne, a U.S. Department of Energy Office of Science Laboratory, is operated under Contract No. DE-AC02-06CH11357. The U.S. Government retains for itself, and others acting on its behalf, a paid-up nonexclusive, irrevocable worldwide license in said article to reproduce, prepare derivative works, distribute copies to the public, and perform publicly and display publicly, by or on behalf of the Government.

* Corresponding author at: Chemical Engineering Division, Argonne National Laboratory, Argonne, IL 60439, USA. Tel.: +1 630 252 3838; fax: +1 630 972 4451.
E-mail address: amine@cmt.anl.gov (K. Amine).
[1] Present address: Energy Business Division Development Team, Samsung SDI Co. Ltd., South Korea.

0378-7753/$ – see front matter © 2007 Elsevier B.V. All rights reserved.
doi:10.1016/j.jpowsour.2007.10.062

hydroxide and oxidized to MnOOH and/or Mn_3O_4 phases. Here, we introduce a coprecipitation method for the preparation of a dense, spherical $(Ni_{1/3}Co_{1/3}Mn_{1/3})CO_3$ carbonate precursor using a continuously stirred tank reactor (CSTR) method. Unlike hydroxide coprecipitation, the carbonate coprecipitation method has the advantage of keeping the oxidation states of Ni, Co, and Mn constant (equal to 2) by the fixation of CO_3^{2-} anion groups. These carbonate precursors were used to obtain dense, spherical, lithium-rich $Li_{1+x}(Ni_{1/3}Co_{1/3}Mn_{1/3})O_2$ materials with different Li contents. The physical and electrochemical properties of these advanced cathode materials are discussed in the light of their morphological, structural, and density characteristics.

2. Experimental approach

Spherical $(Ni_{1/3}Co_{1/3}Mn_{1/3})CO_3$ carbonate precursor was first synthesized by coprecipitation from a solution containing nickel, cobalt, and manganese sulfates by the addition of sodium carbonate solution and ammonia as a chelating agent solution. A 2.0 M aqueous solution of $NiSO_4$, $CoSO_4$, and $MnSO_4$ (Ni:Mn:Co = 1:1:1 molar ratio) was pumped into a CSTR Reactor with a 4-L capacity. At the same time, a 2.0 M aqueous solution of Na_2CO_3 and a 0.2 M NH_4OH solution were independently fed into the reactor. The pH of the solution inside the reactor, maintained at 7.5, was carefully controlled by the addition of the Na_2CO_3 solution. A stirring speed of 1000 rpm was maintained throughout the coprecipitation process. The collected $(Ni_{1/3}Co_{1/3}Mn_{1/3})CO_3$ powder was washed, filtered, and then dried inside an oven at 100 °C for several hours. Stoichiometric amounts of Li_2CO_3 were added to the as-prepared carbonate sample and thoroughly mixed, and then the mix was calcined at 900 °C for 20 h to obtain $Li_{1+x}(Ni_{1/3}Co_{1/3}Mn_{1/3})O_2$ ($0 \le x \le 0.15$) powders. We also obtained these final samples, under the same thermal conditions, by reacting stoichiometric quantities of lithium carbonate and $(Ni_{1/3}Co_{1/3}Mn_{1/3})_3O_4$ oxide. The latter was obtained at 600 °C after the thermal decomposition of the $(Ni_{1/3}Co_{1/3}Mn_{1/3})CO_3$ carbonate precursor.

Powder X-ray diffraction (XRD) patterns of the synthesized materials were collected using a Siemens D5000 diffractometer (Cu Kα radiation). The structural parameters were obtained by the Rietveld refinement method using the FullProf 2000 program [7]. The morphological features and particle size of the elec-

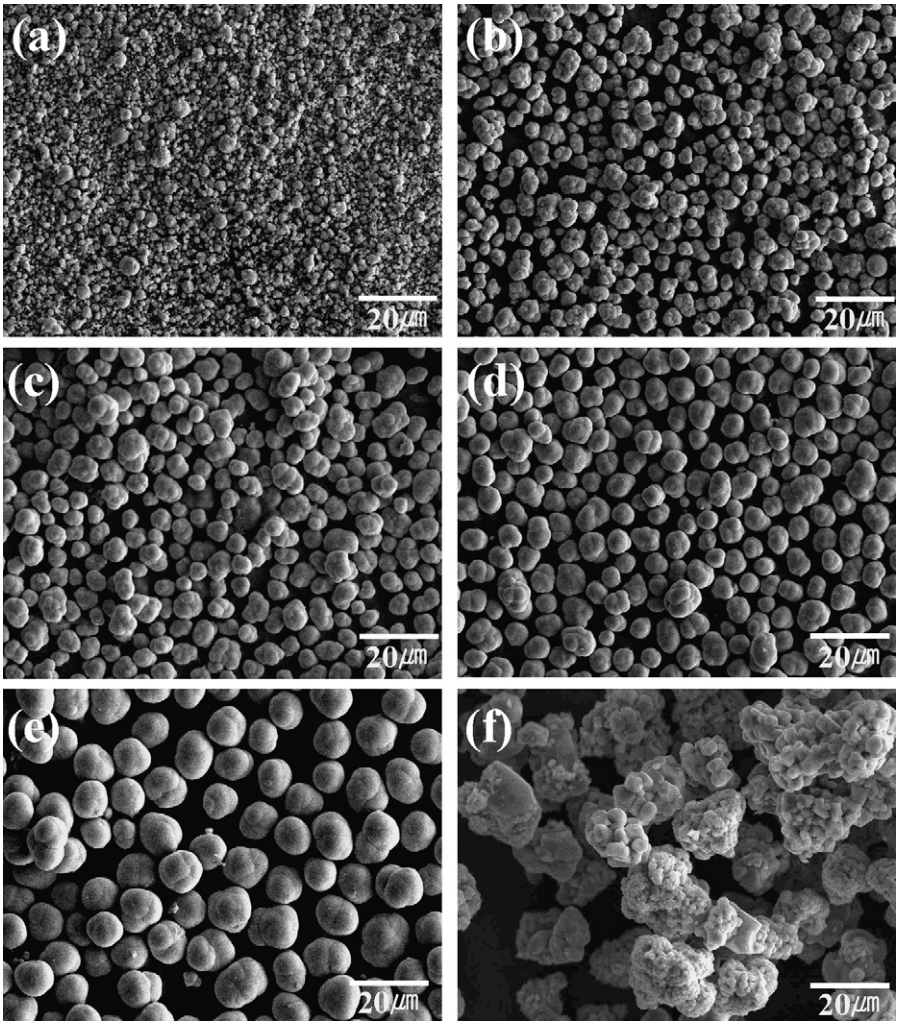

Fig. 1. Scanning electron micrographs of $(Ni_{1/3}Co_{1/3}Mn_{1/3})CO_3$ powder collected at various reaction times: (a) 1 h, (b) 3 h, (c) 5 h, (d) 7 h, (e) 9 h, and (f) 9 h without NH_4OH.

trode powders were analyzed by scanning electron microscopy (SEM) on a JEOL 6400 microscope. Thermal gravimetry (TG) and differential thermal analysis (DTA) were performed using a Seiko EXSTAR 6000 instrument to monitor the weight loss or gain and heat treatment processes under air with a 10 °C min^{-1} heating rate. The electrochemical properties of the Li-rich $Li_{1+x}(Ni_{1/3}Co_{1/3}Mn_{1/3})O_2$ spherical materials and lithium metal and/or MCMB were evaluated using 2032-type coin cells assembled in an argon-filled glove box and tested in room temperature. The positive electrode consisted of 84 wt% oxide powder, 8 wt% carbon conducting additive, and 8 wt% polyvinylidene difluoride (PVDF) binder coated onto an aluminum foil. Metallic lithium foil was used as the negative electrode. The electrolyte consisted of 1.2 M $LiPF_6$ in a 3:7 mixture of ethylene carbonate (EC) and ethyl methyl carbonate (EMC).

3. Results and discussion

Fig. 1 shows the morphologies and particle sizes of the carbonate precursors collected at different times during the precipitation process. In general, many factors affect the morphologies and sizes of the precipitated powders during the precipitation process when a CSTR method is used. These factors include the pH of the solution, the precipitator agent, and the chelating agent. In our case, the pH was fixed at 7.5, the precipitator was Na_2CO_3, and NH_4OH acted as the chelating solution. Under these experimental conditions, the process of making spherical $(Ni_{1/3}Co_{1/3}Mn_{1/3})CO_3$ carbonate precursor started with the formation of small-sized seeds from the agglomeration of primary seeds brought together through their Brownian motion. As the concentration of these seeds increased, secondary particles agglomerated, grew, and took shape by collision and polishing against the baffles and the walls of the reactor [8]. In general, the mechanism of formation for the metal carbonate precursor can be explained according to the following two-step process:

$$(1/3)Ni_{aq}^{2+} + (1/3)Co_{aq}^{2+} + (1/3)Mn_{aq}^{2+} + xNH_4OH_{aq} \rightarrow [Ni_{1/3}Co_{1/3}Mn_{1/3}(NH_3)_n{}^{2+}]_{aq} + (x-n)NH_4OH_{aq} + nH_2O \quad (1)$$

$$[Ni_{1/3}Co_{1/3}Mn_{1/3}(NH_3)_n{}^{2+}]_{aq} + yCO_3{}^{2-} + zH_2O \rightarrow Ni_{1/3}Co_{1/3}Mn_{1/3}(CO_3)_s + zNH_4OH + (n-z)NH_3 \quad (2)$$

This mechanism suggests the formation of an intermediary, ammoniacal mixed transition-metal ligand during the first step. This ligand becomes unstable in the presence of an increasing concentration of carbonic acid, and replacement of the ammoniacal groups takes place during the second step.

To determine the effect of the chelating agent, the precipitation experiment was conducted under the same pH condition in the absence of the NH_4OH solution. The precipitated carbonate sample had irregular particle shapes with random size distribution, as shown in Fig. 1(f). This result clearly shows that the chelating agent NH_4OH plays a major role in obtaining spherical carbonate precursors.

The $(Ni_{1/3}Co_{1/3}Mn_{1/3})CO_3$ carbonate precursor was analyzed by means of TG and DTA measurements to find out the exact phase formation and/or crystallization temperature of the final $Li_{1+x}(Ni_{1/3}Co_{1/3}Mn_{1/3})_{1-x}O_2$ material (Fig. 2). In Fig. 2(a), the TG curve shows two distinguishable weight losses, at about 100 °C and 320 °C, respectively. The first weight loss results

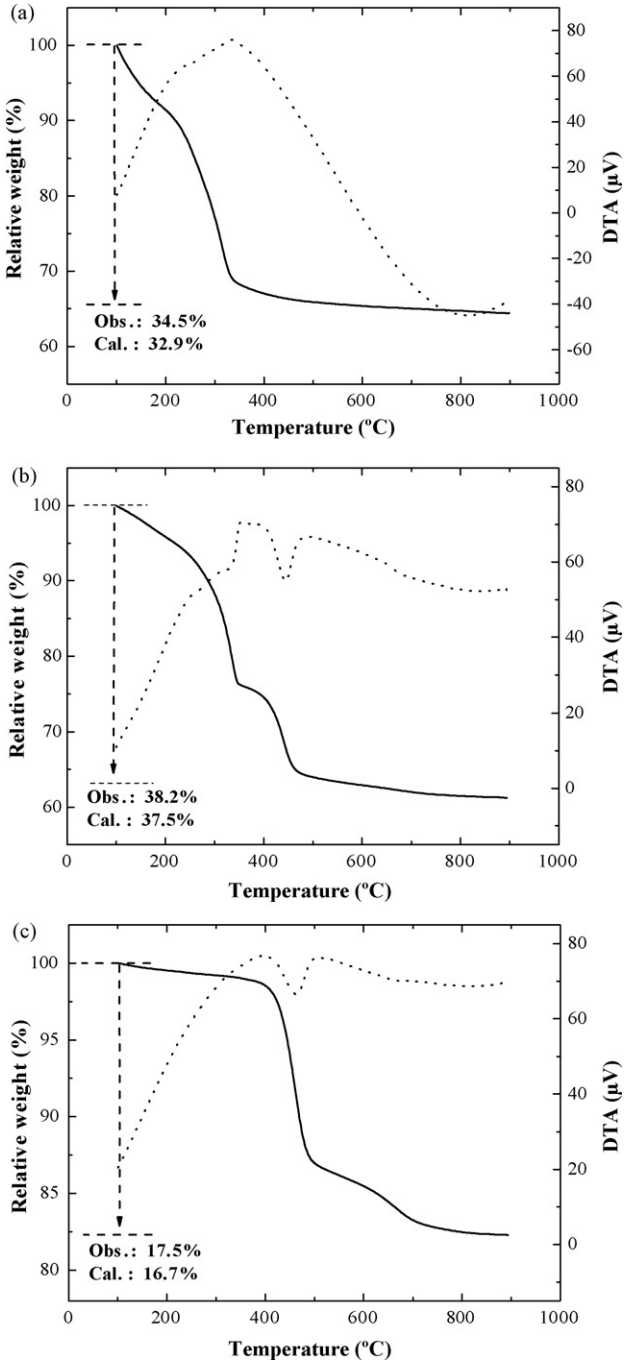

Fig. 2. TG–DTA curves of (a) $(Ni_{1/3}Co_{1/3}Mn_{1/3})CO_3$, (b) Li_2CO_3 and $(Ni_{1/3}Co_{1/3}Mn_{1/3})CO_3$ mixtures, and (c) Li_2CO_3 and $(Ni_{1/3}Co_{1/3}Mn_{1/3})_3O_4$ mixtures.

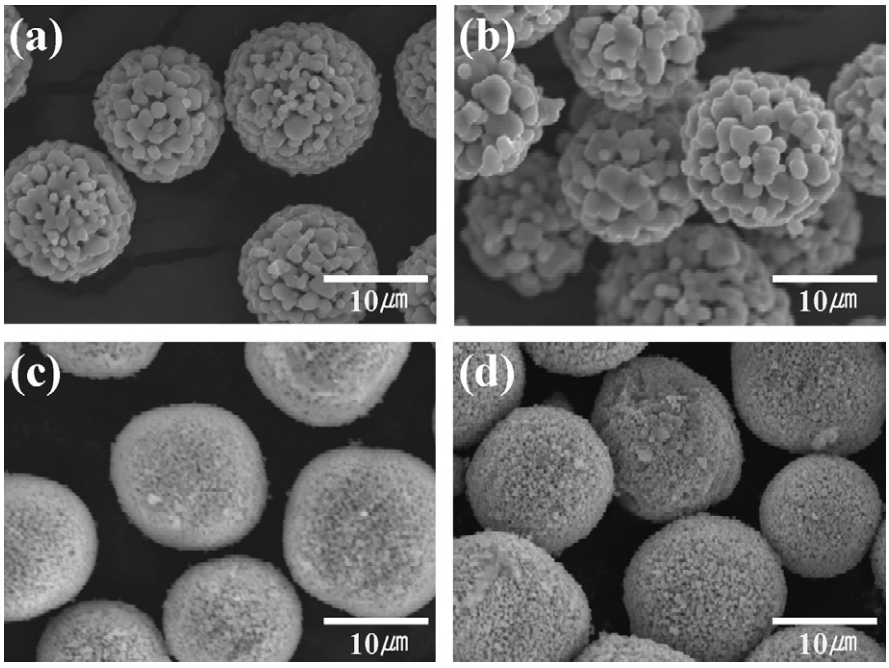

Fig. 3. Scanning electron micrographs for $Li_{1+x}(Ni_{1/3}Co_{1/3}Mn_{1/3})O_2$ powders: (a) and (b) used MCO_3 precursor, $x = 0$–0.15, respectively; (c) and (d) used M_3O_4 precursor, $x = 0$–0.15, respectively.

from the removal of the residual water, while the second one is attributed to decomposition of the carbonate entities. The endothermic transformation that appeared around 320 °C was accompanied by a 34% weight loss, indicating the formation of the $(Ni_{1/3}Co_{1/3}Mn_{1/3})_3O_4$ spinel phase (confirmed by the XRD analysis; see below). Thereafter, further TG–DTA analyzes were conducted on mixtures between Li_2CO_3 and MCO_3 or M_3O_4 ($M = Ni_{1/3}Co_{1/3}Mn_{1/3}$) precursors (Fig. 2(b) and (c)). Within the range of experimental error, the calculated and observed weight losses matched well. In the case of the precalcined M_3O_4 ($M = Ni_{1/3}Co_{1/3}Mn_{1/3}$) spinel precursor, lithium diffusion into its structure occurred at above 500 °C after the decomposition of Li_2CO_3 to develop the layered character of the final material.

Fig. 3 shows SEM photographs of the final $Li_{1+x}(Ni_{1/3}Co_{1/3}Mn_{1/3})O_2$ ($x = 0$ and $x = 0.15$) materials made either from the as-prepared spherical carbonate precursor or after its precalcination at 600 °C. In both cases, the materials were homogeneous and had spherical morphology with good packing properties. We also noticed that after lithiation the size of the secondary particles did not change with respect to the secondary particle size of the carbonate precursor (Figs. 1 and 3). However, the material prepared from $(Ni_{1/3}Co_{1/3}Mn_{1/3})_3O_4$ (Fig. 3(c) and (d)) has much smaller primary particles compared with the material prepared directly from $(Ni_{1/3}Co_{1/3}Mn_{1/3})CO_3$ (Fig. 3(a) and (b)). This result clearly shows that the choice of the mixed transition-metal precursor, whether as an $(Ni_{1/3}Co_{1/3}Mn_{1/3})CO_3$ carbonate or as an $(Ni_{1/3}Co_{1/3}Mn_{1/3})_3O_4$ oxide, is critical in determining the size of the primary particles of the $Li_{1+x}(Ni_{1/3}Co_{1/3}Mn_{1/3})O_2$ materials.

Fig. 4 shows XRD patterns of the $(Ni_{1/3}Co_{1/3}Mn_{1/3})CO_3$ and $(Ni_{1/3}Co_{1/3}Mn_{1/3})_3O_4$ precursors, as well as XRD patterns of the $Li_{1+x}(Ni_{1/3}Co_{1/3}Mn_{1/3})_{1-x}O_2$ materials prepared from the above precursors with various lithium content. Fig. 4(a) shows that the XRD pattern of the coprecipitated carbonate precursor can be indexed on the basis of the hexagonal $R\bar{3}c$ space group usually used for indexing other metal transition compounds, such as $NiCO_3$, $CoCO_3$, and $MnCO_3$. After calcination at 600 °C, the carbonate precursor changed to a spinel-type; the XRD diagram in Fig. 4(b) could be indexed by analogy with the Co_3O_4 spinel material. Moreover, the calcination of the precursor with the lithium salt (Li_2CO_3) resulted in normal layered phases, as seen in Fig. 4(c) and (d). All samples could

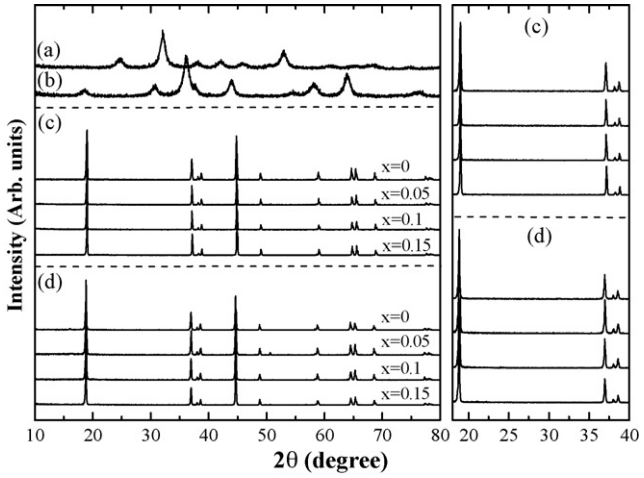

Fig. 4. Powder X-ray diffraction (XRD) patterns of (a) as-prepared $(Ni_{1/3}Co_{1/3}Mn_{1/3})CO_3$; (b) precalcined at 600 °C, $(Ni_{1/3}Co_{1/3}Mn_{1/3})_3O_4$; (c) and (d) are for $Li_{1+x}(Ni_{1/3}Co_{1/3}Mn_{1/3})O_2$ used by (a) and (b) precursor, respectively.

Table 1
Crystallographic data and tap densities obtained by Rietveld refinements and tapping machine, respectively

x in $Li_{1+x}(M)O_2$	Lattice constant (A)		$I(0\,0\,3/1\,0\,4)$	R_{wp} (%)	Cation mixing Ni in Li site	Tap density (g mL^{-1})
	a_h	c_h				
I						
$x=0.00$	2.859(4)	14.242(0)	1.08	10.6	0.04(3)	1.70
$x=0.05$	2.859(8)	14.232(9)	1.15	11.3	0.03(7)	1.66
$x=0.10$	2.858(3)	14.226(1)	1.24	10.2	0.01(8)	1.45
$x=0.15$	2.846(7)	14.144(1)	1.25	12.4	0.01(5)	1.40
II						
$x=0.00$	2.860(5)	14.247(6)	1.10	10.4	0.05(5)	1.72
$x=0.05$	2.854(6)	14.243(8)	1.14	10.6	0.04(3)	1.76
$x=0.10$	2.853(4)	14.189(5)	1.25	11.7	0.02(2)	1.82
$x=0.15$	2.850(6)	14.245(3)	1.49	12.5	0.01(7)	1.65

be indexed on the basis of a hexagonal α-$NaFeO_2$ structure with the space group $R\bar{3}m$ (No. 166). Recently, Kim et al. reported that lithium-rich $Li_{1+x}(Ni_{1/3}Co_{1/3}Mn_{1/3})_{1-x}O_2$ materials can be prepared by a spray-drying method [6]. However, their materials showed a small number of impurity peaks between 20° and 23° (2θ), probably due to the Li_2MnO_3 super-lattice ordering [9]. In this study, there was no evidence of such super-lattice ordering peaks by XRD. However, some of us recently reported a small amount of Li_2MnO_3 phase that was indentified using NMR spectrum [10]. It is proposed that the addition of Co^{3+} to the transition-metal layers in the $Li_{1+x}[Mn_{1/3}Ni_{1/3}Co_{1/3}]_{1-x}O_2$ compounds at the expense of Mn^{4+} and Ni^{2+} reduces the amount and size of the Li_2MnO_3-like regions, compared with $Li_{1+x}[Ni_{1/2}Mn_{1/2}]_{1-x}O_2$ compounds [9,10]. In addition, the clear splitting of the (0 0 6)/(1 0 2) and (1 0 8)/(1 1 0) doublets with increased lithium content suggests that this materials has a good crystallinity and a well-ordered layered structure [11].

The structures of $Li_{1+x}(Ni_{1/3}Co_{1/3}Mn_{1/3})_{1-x}O_2$ ($x=0$–0.15) materials were investigated by the Rietveld refinement method. Table 1 shows a summary of the crystallographic parameters obtained from the Rietveld results. The refinements were carried out assuming an α-$NaFeO_2$-type hexagonal structure ($R\bar{3}m$), in which Li ions occupy the 3b (0,0,1/2) site; Ni, Mn, and Co are located in the 3a (0,0,0) site; and O is located in the 6c (0,0,z_{oxy}) site (z_{oxy} is close to 1/4). The degree of cation mixing between lithium and nickel was calculated, with the assumption that some nickel ions might occupy the lithium site because the radius of Ni^{2+} (0.69 Å) is close to that of Li^+ (0.76 Å). As a result, when the lithium content increases, the extent of the mixing between lithium and nickel becomes less, indicating that cationic mixing could be prohibited by an excess of lithium ions. The variation of the lattice constants a and c, and the $I(0\,0\,3)/I(1\,0\,4)$ intensity ratio of all $Li_{1+x}(Ni_{1/3}Co_{1/3}Mn_{1/3})O_2$ ($0 \le x \le 0.15$) materials, are also summarized in Table 1. We also observed that the $I(0\,0\,3)/I(1\,0\,4)$ intensity ratio increased when the lithium con-

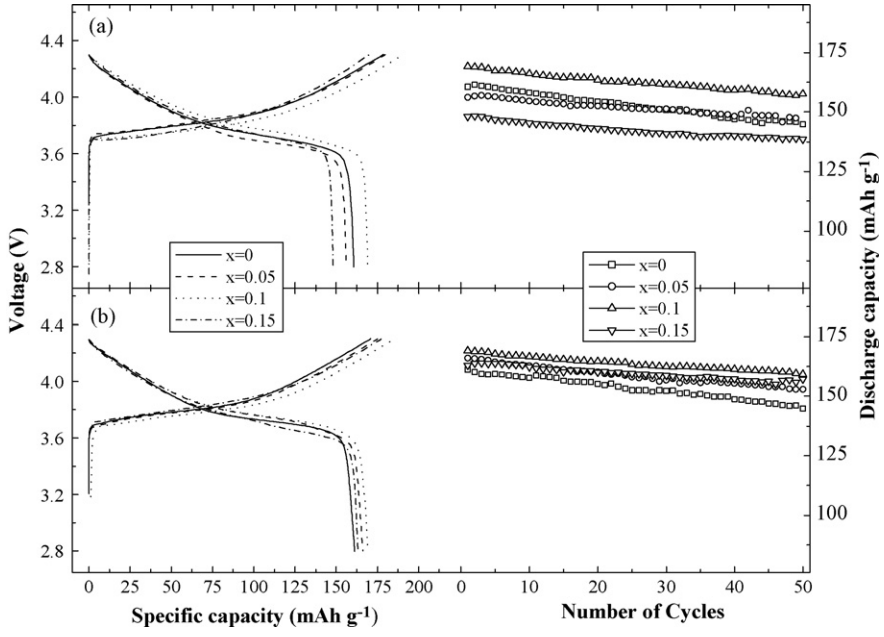

Fig. 5. Charge/discharge voltage profiles and discharge capacity for (a) as-prepared $(Ni_{1/3}Co_{1/3}Mn_{1/3})CO_3$ and (b) precalcined at 600 °C, $(Ni_{1/3}Co_{1/3}Mn_{1/3})_3O_4$ used materials, and Li/$Li_{1+x}(Ni_{1/3}Co_{1/3}Mn_{1/3})O_2$ cells.

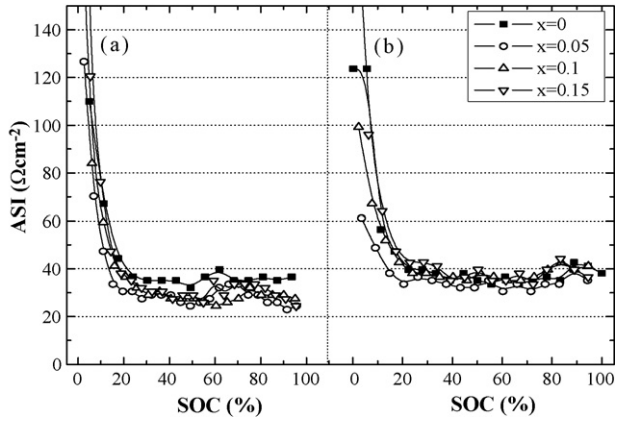

Fig. 6. Area specific impedance (ASI) vs. state of charge (SOC) for C/$Li_{1+x}(Ni_{1/3}Co_{1/3}Mn_{1/3})O_2$ cells: (a) as-prepared $(Ni_{1/3}Co_{1/3}Mn_{1/3})CO_3$ and (b) precalcined at 600 °C, $(Ni_{1/3}Co_{1/3}Mn_{1/3})_3O_4$ used materials, respectively.

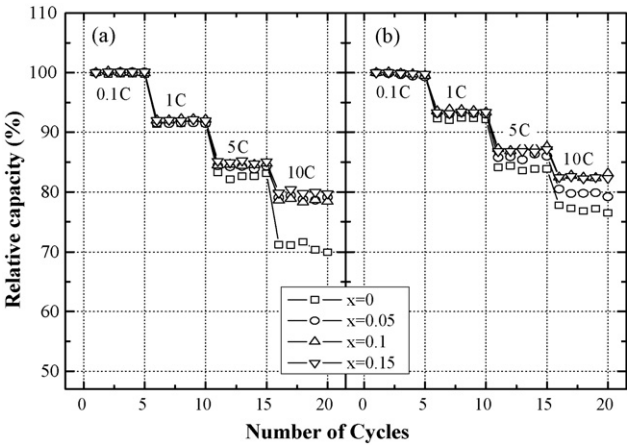

Fig. 7. Variation of rate capability with relative capacity for C/$Li_{1+x}(Ni_{1/3}Co_{1/3}Mn_{1/3})O_2$ cells; materials were prepared with (a) as-prepared $(Ni_{1/3}Co_{1/3}Mn_{1/3})CO_3$ and (b) precalcined at 600 °C, $(Ni_{1/3}Co_{1/3}Mn_{1/3})_3O_4$ precursor. The cell was charged/discharged between 2.8 and 4.2 V at room temperature.

tent increased, which means that the $Li_{1+x}(Ni_{1/3}Co_{1/3}Mn_{1/3})O_2$ materials have a more pronounced layered character when extra lithium is introduced into their structures. These observations are in agreement with previous reports in the literatures [12,13].

Fig. 5 shows charge/discharge curves and cycling properties for the Li/$Li_{1+x}(Ni_{1/3}Co_{1/3}Mn_{1/3})O_2$ cells containing different Li-rich $Li_{1+x}(Ni_{1/3}Co_{1/3}Mn_{1/3})O_2$ ($x = 0$–0.15) materials. The cells were cycled between 2.8 and 4.3 V at room temperature in a constant-current mode with a current density of 0.1 mA cm^{-2}. We noticed that when the lithium content increased, the discharge capacities increased (up to 10%) and cycling properties were improved. These results were expected, because our structural study showed that the materials had better lamellar character, with less cationic mixing, when the lithium concentration was higher.

Fig. 6 shows the area specific impedance (ASI) of the C/$Li_{1+x}(Ni_{1/3}Co_{1/3}Mn_{1/3})O_2$ ($x = 0$–0.15) cells as a function of the state of charge (SOC), with a 30-s current interruption every 30 min. During lithium ion intercalation/de-intercalation, a combination of electrode polarization, ohmic drop, and diffusion of Li^+ ions through the electrolyte and of solid-state lithium ions within the electrode caused the overall cell voltage to change [14]. In our previous study, the ASI values of the Li$(Ni_{1/3}Co_{1/3}Mn_{1/3})O_2$ materials showed that they could be used for high-power battery applications [15]. In this study, the samples with increased lithium content tended to show slightly lower ASI values when compared with the materials having no excess lithium ions. These results could be attributed to the small degree of cationic mixing and also to the existence of Ni^{3+} ions, which could have improved the electronic conductivity of the materials with higher lithium content [16].

Fig. 7 shows the rate capability properties of C/$Li_{1+x}(Ni_{1/3}Co_{1/3}Mn_{1/3})O_2$ cells tested with various applied currents in room temperature. All samples operated initially for five cycles at a current density of 0.1 mA cm^{-2} (16 mA g^{-1}, 0.1 C). The charge current density was kept constant at 1 mA cm^{-2} (160 mA g^{-1}, 1 C) for the rate capability tests that followed. However, the discharge capacity changed from 1 to 4, and then to 7 mA cm^{-2}, which corresponded to 160 mA g^{-1} (1 C), 640 mA g^{-1} (5 C), and 1120 mA g^{-1} (10 C), respectively. As shown in Fig. 7, when the lithium content was increased, the rate capability properties were significantly improved, as well as the cycling behavior. Moreover, the $Li_{1+x}(Ni_{1/3}Co_{1/3}Mn_{1/3})O_2$ materials that were made from the $(Ni_{1/3}Co_{1/3}Mn_{1/3})_3O_4$ oxide precursor showed even better rate capability properties than those of the material made from the carbonate $(Ni_{1/3}Co_{1/3}Mn_{1/3})CO_2$ samples. For instance, the electrode fabricated with the $Li_{1+x}(Ni_{1/3}Co_{1/3}Mn_{1/3})O_2$ ($x = 0.1$, 0.15) materials showed excellent rate capability even at a 10 C rate (1120 mA g^{-1}), as shown in Fig. 7(b). In this case, the discharge capacity obtained was about 82% of the capacity measured at 0.1 C (16 mA g^{-1}), which testifies to excellent performance under higher current densities than those in previous reports [17,18]. This enhanced discharge capacity at accelerated rates clearly demonstrates the advantages of the spherical carbonate precursor. As shown in the SEM photographs in Fig. 3, the secondary particles of precalcined precursors are composed of nano-size primary particles, with high enough porosity to allow for better electrolyte wettability. Similar improvements in electrochemical properties by nano-size grains have been previously reported [19–21]. Therefore, we consider that the high rate capability properties of Li-rich $Li_{1+x}(Ni_{1/3}Co_{1/3}Mn_{1/3})O_2$ materials make them suitable for potential application in high-power lithium-ion batteries.

4. Conclusions

Spherical Li-rich $Li_{1+x}(Ni_{1/3}Co_{1/3}Mn_{1/3})O_2$ materials have been prepared from Li_2CO_3 and coprecipitated $(Ni_{1/3}Co_{1/3}Mn_{1/3})CO_3$ or precalcined $(Ni_{1/3}Co_{1/3}Mn_{1/3})_3O_4$ precursors and evaluated in lithium cells. The thermogravimetric, structural, morphological, and electrochemical properties of these $Li_{1+x}(Ni_{1/3}Co_{1/3}Mn_{1/3})O_2$ materials were investigated by TG, XRD, SEM, and galvanostatic cycling for all lithium contents. As the lithium content was increased, we observed not only a well-ordered layered structure, but also better cycling

properties, lower ASI values, and remarkable improvements in rate capability. These results might be related to the lessened extent of cationic mixing, the narrow size distributions and spherical morphology of the secondary particles with smaller crystallites, and the absence of impurities.

Acknowledgments

This research was funded by the U.S. Department of Energy, FreedomCAR and Vehicle Technologies Office. Argonne National Laboratory is operated for the U.S. Department of Energy by UChicago Argonne, LLC, under contract DE-AC0Z-06CH11357.

References

[1] T. Ohzuku, Y. Makimura, Chem. Lett. 7 (2001) 642.
[2] N. Yabuuchi, T. Ohzuku, J. Power Sources 119–121 (2003) 171.
[3] W. Lu, Z. Chen, H. Joachin, J. Prakash, J. Liu, K. Amine, J. Power Sources 3 (2007) 1074–1079.
[4] Y.M. Todorov, K. Numata, Electrochim. Acta 50 (2004) 495.
[5] Z. Lu, D.D. MacNeil, J.R. Dahn, Electrochem. Solid State Lett. 4 (2001) A200.
[6] J.-M. Kim, N. Kumagai, H.-T. Chung, Electrochem. Solid State Lett. 9 (11) (2006) A494.
[7] T. Roisnel, J. Rodriguez-Carjaval, Fullprof Manual, Institute Laue-Langevin, Grenoble, 2000.
[8] J.W. Mullin, Crystallization, Butterworths, London, 1961.
[9] W.-S. Yoon, S. Iannopollo, C.P. Grey, D. Carlier, J. Gorman, J. Reed, G. Ceder, Electrochem. Solid State Lett. 7 (7) (2004) A167.
[10] M.M. Thackeray, S.-H. Kang, C.S. Johnson, J.T. Vaughey, S.A. Hackney, Electrochem. Commun. 8 (2006) 1531.
[11] A. Rougier, P. Gravereau, C. Delmas, J. Electrochem. Soc. 143 (4) (1996) 1168.
[12] S. Jouanneau, K.W. Eberman, L.J. Krause, J.R. Dahn, J. Electrochem. Soc. 150 (12) (2003) A1637.
[13] S.W. Oh, S.-H. Park, C.-W. Park, Y.-K. Sun, Solid State Ionics 171 (2004) 167–172.
[14] Q. Wu, W. Lu, J. Prakash, J. Power Sources 88 (2000) 237.
[15] I. Belharouak, Y.-K. Sun, J. Liu, K. Amine, J. Power Sources 123 (2003) 247.
[16] J.-M. Kim, H.-T. Chung, Electrochim. Acta 49 (2004) 3573.
[17] D.-C. Li, T. Muta, L.-Q. Zhang, J. Power Sources 132 (2004) 150.
[18] J. Guo, L.F. Jiao, H.T. Yuan, H.X. Li, M. Zhang, Y.M. Wang, Electrochim. Acta 51 (2006) 3731.
[19] S.-H. Kang, J.B. Goodenough, L.K. Rabenberg, Chem. Mater. 13 (2001) 1758.
[20] A.R. Armstrong, A.J. Paterson, A.D. Robertson, P.G. Bruce, Chem. Mater. 14 (2002) 710.
[21] S.-H. Park, H.-S. Shin, S.-T. Myung, C.S. Yoon, K. Amine, Y.-K. Sun, Chem. Mater. 17 (2005) 6.